

Distributed component-level modeling and control of energy dynamics in electric power systems [★]

Hiya Gada ^a, Rupamathi Jaddivada, Marija Ilic ^a

^aLaboratory for Information and Decision Systems, Massachusetts Institute of Technology, Cambridge, MA 02139, USA

Abstract

The widespread deployment of power electronic-based technologies is transforming modern power systems into fast, nonlinear, and heterogeneous systems. Conventional modeling and control approaches, rooted in quasi-static analysis and centralized control, are inadequate for these converter-dominated systems, which operate on fast timescales and involve proprietary models of diverse components. This paper adopts and extends a previously introduced energy space modeling framework grounded in energy conservation principles to address these challenges. We generalize the notion of a *port interaction variable*, which encodes energy exchange between interconnected, heterogeneous components in a unified and physically intuitive manner. A multilayered distributed control architecture is proposed, wherein the nonlinear physical dynamics of each component are lifted to a higher-level linear energy space through well-defined mappings. Distributed controllers are designed in this energy space using only local states and minimal neighbor information via port interaction variables. Two control designs, energy-based feedback linearizing control (FBLC) and sliding mode control (SMC), are proven to achieve asymptotic convergence to reference outputs. The approach is validated on two systems: an inverter-controlled RLC circuit and a synchronous generator connected to a load. In both cases, energy-based control improves transient response and reduces control effort.

Key words: energy dynamics, generalized reactive power, interaction variable, distributed control, feedback linearizing control (FBLC), sliding mode control (SMC), inverter-based control

1 Introduction

Modern electric power systems are rapidly evolving with the integration of power electronic technologies, including inverter-based resources (IBRs), battery energy storage systems (BESS), high-voltage direct current (HVDC) links, and flexible alternating current transmission systems (FACTS) [1,2,3]. These devices operate at fast timescales and rely on embedded control algorithms to govern their dynamics behavior. Traditional modeling and control frameworks rely on approximations such as quasi-static phasor representations and PQ decoupling [4,5]. However, these approximations are increasingly invalid in systems dominated by fast, nonlinear, and tightly coupled converter dynamics [6].

Moreover, most components in modern power systems, including inverters, power converters, and synchronous

generators, exhibit inherently nonlinear dynamics [7,8]. Controllers for these systems are based on nonlinear feedback tailored to the specific technologies involved [9]. While effective at the component level, these methods rarely offer general system-level guarantees due to cross-couplings and unmodeled interactions [10,11]. Unlike linear systems, nonlinear systems lack general stability and controllability certificates, making control coordination and analysis more complex. This highlights the need for modeling and control frameworks that can accommodate both conventional and converter-based nonlinear dynamics, while providing system-level stability guarantees.

Compounding these challenges is the increasing heterogeneity of the modern grid. Components are often developed by different vendors and rely on proprietary modeling, control algorithms, and communication protocols, which limits observability and makes centralized coordination infeasible [11]. The co-existence of synchronous generators, grid-forming (GFM) inverters, and grid-following (GFL) inverters, each governed by distinct control paradigms and timescales, demands new abstractions that can unify component dynamics in a modular and heterogeneity-resilient manner [10,12]. Re-

[★] This paper was not presented at any IFAC meeting. Corresponding author Hiya Gada. Tel. +1-857-468-9301

Email addresses: hiyagada@mit.edu (Hiya Gada),
jrupamathi93@gmail.com (Rupamathi Jaddivada),
ilic@mit.edu (Marija Ilic).

cent work has shown that distributed control architectures offer a promising pathway by enabling local control decisions using only local measurements and minimum peer-to-peer communication, while still achieving global objectives such as frequency regulation [13]. Additionally, distributed control eliminates the need for global observability or full model knowledge, significantly reducing computational complexity and enhancing scalability in large, modular systems.

While distributed control addresses limitations of centralized architectures, its effectiveness depends on the underlying modeling framework. This work adopts and builds upon prior work in energy space modeling [14,15,16] grounded in the first principles of energy conservation and system interconnection. Unlike traditional state-space models that use voltage and current as state variables, energy space uses physically intuitive variables, such as energy and power, providing a unified framework for system representation. The resulting energy dynamic equations are linear in the energy state and input variables, facilitating control design and stability analysis. Defined entirely in the time domain, the framework effectively captures fast electromagnetic transients and inverter dynamics. Moreover, energy space models are constructed at the component level and support modular and scalable architectures, aligning naturally with distributed control frameworks [17].

A central construct within energy space modeling is the notion of a *port interaction variable*, which captures energy exchange between subsystems via shared ports. These variables are defined based on energy/power flows, independent of component technology, facilitating distributed control design that is inherently technology agnostic. Over the last two decades, the interaction variable-based theory has been extended and utilized to design nonlinear controllers, including control of power electronic-based inverters, induction machines, generators, and residential demand-side technologies [18,19,20]. This work builds on these foundations to formulate a distributed control problem in energy space and develop controllers that are compatible with fast, nonlinear, heterogeneous component dynamics.

Section 2 formulates a general distributed control problem for an interconnected power system modeled as a set of subsystems with local dynamics subject to port, control, and exogenous inputs. A common output exchanged between subsystems encodes physical interconnections and defines local control objectives. The control objective is to design local controllers that achieve output reference tracking while satisfying interconnection constraints. Section 3 reviews the energy space modeling framework used throughout the paper. We summarize preliminaries from previous work [14,15,16], then introduce an extended third-order energy space model that captures both the stored energy dynamics and the dynamics of stored energy in tangent space,

previously treated as an independent disturbance. This extension improves modeling of fast-timescale behavior and enhances control design. Section 4 focuses on the design of distributed controllers within the energy space framework. It establishes a multilayered structure in which each component's physical dynamics are lifted to energy space via well-defined mappings. This formulation enables the distributed control problem to be posed in energy space using the port interaction variable as the minimal information exchanged between subsystems. Two controllers are developed, energy-based feedback linearizing control (FBLC) and sliding mode control (SMC), and sufficient conditions for asymptotic output convergence are established. Section 6 demonstrates the proposed modeling and control designs through two examples. The first is an RLC circuit with an inverter-controlled voltage source, and the second is a synchronous machine, with voltage and frequency regulation as their respective control objectives. The proposed controllers show improved transient performance and reduced control effort compared to conventional methods. Finally, Section 7 presents concluding remarks and directions for future work.

2 Distributed control problem formulation

To formally pose the distributed control problem, we begin by reviewing the modeling approach presented in [21], which represents the overall system as an interconnection of subsystems or components, as illustrated in Figure 1. Let $x_i \in \mathcal{X}_i$, $u_i \in \mathcal{U}_i$, $r_i \in \mathcal{R}_i$ and $m_i \in \mathcal{M}_i$ denote the state variables, control inputs, port inputs and exogenous disturbances of component Σ_i , respectively. Each component can be analyzed in isolation by introducing shared variables at the interface, captured by the port inputs r_i , which encode the interaction between the component and the rest of the system.

The dynamic model of stand-alone component Σ_i is described by the set of equations in (1). Without loss of generality, we assume that the control input u_i , port input r_i , and exogenous input m_i enter affinely in the state dynamics through state-dependent input functions.

$$\text{Initial condition: } x_i(0) = x_{i,0} \quad (1a)$$

State dynamics:

$$\dot{x}_i = f_{x,i}(x_i) + g_i^r(x_i) r_i + g_i^m(x_i) m_i + g_i^u(x_i) u_i \quad (1b)$$

$$\text{Output of interest: } y_i = f_{y,i}(x_i, u_i, r_i, m_i) \quad (1c)$$

$$\text{Common output: } z_i = f_{z,i}(x_i, u_i, r_i, m_i) \quad (1d)$$

Here, y_i represents the component's output of interest for which local control is being designed. The variable z_i represents the common output that is physically shared between neighboring components through interconnection.

Physical consistency at the interface between neighbor-

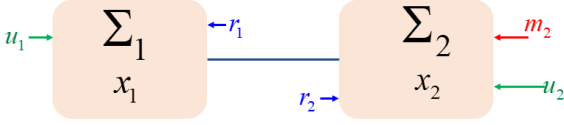


Fig. 1. Interconnected system comprising two components Σ_1 and Σ_2 with local controllable input u_1, u_2 and exogenous disturbances m_2

ing components, i.e., ensuring that the overall system can physically exist and operate, imposes a feasibility constraint on the shared common outputs of interconnected subsystems. This constraint typically arises from conservation laws, such as generalized Tellegen's theorem [22] in electrical networks.

The primary difficulty in distributed control problem is to be able to find consistent relations between control specifications on y_i and common output variables z_j communicated by neighboring components Σ_j . Assuming one can find such a map ψ_i of the form in (2), the output reference can be given as,

$$y_i^{ref} = \psi_i(x_i, z_j), \quad \forall j \in \mathcal{C}_i \quad (2)$$

where \mathcal{C}_i denotes the set of components that are directly connected to Σ_i (i.e., its neighbors). The distributed control problem is formally posed in Problem 1, where the control objective is to ensure that the output tracks its reference, subject to the feasibility constraint imposed by interconnection interfaces.

Problem 1 (Distributed control problem formulation). *Given a system consisting of a set \mathcal{N} of interconnected subsystems, the goal is to design a smooth feedback control law of the form,*

$$u_i = c_i(x_i, z_j, y_i^{ref}), \quad j \in \mathcal{C}_i, \quad \forall i \in \mathcal{N}$$

that utilizes local state information x_i and minimal information z_j communicated by neighboring components Σ_j , such that the following feasibility constraint is satisfied and the control objective is achieved:

- (1) *Feasibility constraint: For each interconnection, the common output variables of neighboring components must satisfy,*

$$z_i = - \sum_{j \in \mathcal{C}_i} z_j, \quad \forall i \in \mathcal{N}$$

- (2) *Control objective: The local output of interest y_i must track a consistent reference given by the map ψ_i as defined in (2),*

$$y_i \rightarrow y_i^{ref} \quad \text{as } t \rightarrow \infty, \quad \forall i \in \mathcal{N}$$

3 Energy-based modeling of a component

To enable a physically intuitive understanding of system behavior, effectively characterize heterogeneous technologies, and facilitate time-domain analysis, we map the conventional state dynamics of a component into an *energy space* where the system dynamics become linear.

3.1 Preliminaries

Definition 1 (Stored energy). *The stored energy of component Σ_i is described by the energy function $E_i : \mathcal{X}_i \rightarrow \mathbb{R}$, defined as,*

$$E_i(x_i) = \frac{1}{2} x_i^\top H_i(x_i) x_i,$$

where $H_i(x_i)$ is a positive definite symmetric matrix for all $x_i \in \mathcal{X}_i$.

Stored energy is defined by the inertia matrix $H_i(x_i)$, representing inductance/capacitance in electrical systems and mass/inertia in mechanical systems. Its properties and physical interpretations are detailed in [14,23].

Definition 2 (Stored energy in tangent space). *For the same positive definite matrix H_i as in Definition 1, the stored energy in tangent space $E_{t,i}$ is defined over the tangent bundle $\mathcal{T}\mathcal{X}_i$, where $(x_i, \dot{x}_i) \in \mathcal{T}\mathcal{X}_i$, through the mapping $E_{t,i} : \mathcal{T}\mathcal{X}_i \rightarrow \mathbb{R}$ as,*

$$E_{t,i}(x_i, \dot{x}_i) = \frac{1}{2} \dot{x}_i^\top H_i(x_i) \dot{x}_i.$$

Definition 3 (Power dissipation). *The instantaneous power dissipated by the component Σ_i is described by a dissipation function $D_i : \mathcal{X}_i \rightarrow \mathbb{R}$, defined as,*

$$D_i(x_i) = \frac{1}{2} x_i^\top B_i(x_i) x_i$$

where $B_i(x_i)$ is a positive semi-definite matrix for all $x_i \in \mathcal{X}_i$.

Definition 4 (Power dissipation in tangent space). *For the same positive semi-definite matrix $B_i(x_i)$, as in Definition 3, the instantaneous power dissipated in tangent space by the component Σ_i is described by a dissipation function $D_{t,i} : \mathcal{T}\mathcal{X}_i \rightarrow \mathbb{R}$, defined as,*

$$D_{t,i}(x_i, \dot{x}_i) = \frac{1}{2} \dot{x}_i^\top B_i(x_i) \dot{x}_i$$

Definition 5 (Time constant). *The time constant of component Σ_i at state x_i is defined as,*

$$\tau_i(x_i) = \frac{E_i(x_i)}{D_i(x_i)}$$

provided that $D_i(x_i) > 0$.

Definition 6 (Time constant in tangent space). *The time constant in tangent space of component Σ_i , at states (x_i, \dot{x}_i) is defined as,*

$$\tau_{t,i}(x_i, \dot{x}_i) = \frac{E_{t,i}(x_i, \dot{x}_i)}{D_{t,i}(x_i, \dot{x}_i)}$$

provided that $D_{t,i}(x_i, \dot{x}_i) > 0$.

We formalize port, control, and disturbance inputs using the concept of effort and flow variables. Let \mathcal{E}_i and \mathcal{F}_i denote dual vector spaces such that $\mathcal{E}_i = (\mathcal{F}_i)^*$ and $\mathcal{F}_i = (\mathcal{E}_i)^*$. We refer to elements $e_i \in \mathcal{E}_i$ and $f_i \in \mathcal{F}_i$ as effort and flow variables, respectively [24]. Effort variables represent generalized forces (e.g., voltage, mechanical force), while flow variables denote their conjugates (e.g., current, velocity). The generalized real power, rate of change of reactive power, and tangent-space power associated with each input are defined via these variables.

Definition 7 (Instantaneous power). *The instantaneous power P_i^r injected into a component Σ_i at the port is given by the mapping $P_i^r : \mathcal{E}_i^r \times \mathcal{F}_i^r \rightarrow \mathcal{P}_i^r$ and is defined as,*

$$P_i^r = e_i^r f_i^r$$

where $e_i^r \in \mathcal{E}_i^r$ and $f_i^r \in \mathcal{F}_i^r$ respectively represent the effort and flow variables at the port of interconnection. Similarly, instantaneous power contributions from control and disturbance inputs are given by the mappings,

$$P_i^u : \mathcal{E}_i^u \times \mathcal{F}_i^u \rightarrow \mathcal{P}_i^u, \quad P_i^m : \mathcal{E}_i^m \times \mathcal{F}_i^m \rightarrow \mathcal{P}_i^m$$

and is defined as,

$$\begin{aligned} P_i^u &= e_i^u f_i^u, \\ P_i^m &= e_i^m f_i^m, \end{aligned}$$

with $e_i^u \in \mathcal{E}_i^u$, $f_i^u \in \mathcal{F}_i^u$ and $e_i^m \in \mathcal{E}_i^m$, $f_i^m \in \mathcal{F}_i^m$ denoting the effort and flow variables associated with the control and disturbance inputs, respectively.

Definition 8 (Rate of change of generalized reactive power). *The rate of change of generalized reactive power \dot{Q}_i^r injected into a component Σ_i at the port is given by the mapping $\dot{Q}_i^r : \mathcal{T}\mathcal{E}_i^r \times \mathcal{T}\mathcal{F}_i^r \rightarrow \mathcal{T}\mathcal{Q}_i^r$ and is defined as,*

$$\dot{Q}_i = e_i^r \frac{df_i^r}{dt} - f_i^r \frac{de_i^r}{dt}$$

where $(e_i^r, \dot{e}_i^r) \in \mathcal{T}\mathcal{E}_i$ and $(f_i^r, \dot{f}_i^r) \in \mathcal{T}\mathcal{F}_i$ denote the tangent bundles of the effort and flow spaces at the port. Analogously, we define the rate of change of generalized reactive power contributed by control and disturbance inputs through the mappings,

$$\dot{Q}_i^u : \mathcal{T}\mathcal{E}_i^u \times \mathcal{T}\mathcal{F}_i^u \rightarrow \mathcal{T}\mathcal{Q}_i^u, \quad \dot{Q}_i^m : \mathcal{T}\mathcal{E}_i^m \times \mathcal{T}\mathcal{F}_i^m \rightarrow \mathcal{T}\mathcal{Q}_i^m$$

with,

$$\begin{aligned} \dot{Q}_i^u &= e_i^u \frac{df_i^u}{dt} - f_i^u \frac{de_i^u}{dt} \\ \dot{Q}_i^m &= e_i^m \frac{df_i^m}{dt} - f_i^m \frac{de_i^m}{dt} \end{aligned}$$

where $(e_i^u, \dot{e}_i^u) \in \mathcal{T}\mathcal{E}_i^u$, $(f_i^u, \dot{f}_i^u) \in \mathcal{T}\mathcal{F}_i^u$ are the control input tangent bundles and $(e_i^m, \dot{e}_i^m) \in \mathcal{T}\mathcal{E}_i^m$, $(f_i^m, \dot{f}_i^m) \in \mathcal{T}\mathcal{F}_i^m$ are their disturbance counterparts.

Definition 9 (Instantaneous power in tangent space). *The instantaneous power in tangent space $P_{t,i}^r$ into a component Σ_i at the port is given by the mapping $P_{t,i}^r : T_{e_i^r}\mathcal{E}_i^r \times T_{f_i^r}\mathcal{F}_i^r \rightarrow \mathcal{P}_{t,i}^r$ and is defined as,*

$$P_{t,i}^r = \frac{de_i^r}{dt} \frac{df_i^r}{dt}$$

where $\dot{e}_i^r \in T_{e_i^r}\mathcal{E}_i^r$ and $\dot{f}_i^r \in T_{f_i^r}\mathcal{F}_i^r$ respectively represent the time derivatives of the effort and flow variables at the port of interconnection. Similarly, instantaneous power in tangent space from control and disturbance inputs are given by the mappings,

$$\begin{aligned} P_{t,i}^u &: T_{e_i^u}\mathcal{E}_i^u \times T_{f_i^u}\mathcal{F}_i^u \rightarrow \mathcal{P}_{t,i}^u, \\ P_{t,i}^m &: T_{e_i^m}\mathcal{E}_i^m \times T_{f_i^m}\mathcal{F}_i^m \rightarrow \mathcal{P}_{t,i}^m, \end{aligned}$$

and are defined as,

$$\begin{aligned} P_{t,i}^u &= \dot{e}_i^u \dot{f}_i^u, \\ P_{t,i}^m &= \dot{e}_i^m \dot{f}_i^m, \end{aligned}$$

with $\dot{e}_i^u \in T_{e_i^u}\mathcal{E}_i^u$, $\dot{f}_i^u \in T_{f_i^u}\mathcal{F}_i^u$ and $\dot{e}_i^m \in T_{e_i^m}\mathcal{E}_i^m$, $\dot{f}_i^m \in T_{f_i^m}\mathcal{F}_i^m$ denoting the time derivatives of the effort and flow variables associated with the control and disturbance inputs, respectively.

For the port interaction terms $(P_i^r, \dot{Q}_i^r, P_{t,i}^r)$, the associated effort and flow variables depend on both the internal state and the port input, i.e.,

$$e_i^r = \varepsilon_i^r(x_i, r_i), \quad f_i^r = \zeta_i^r(x_i, r_i), \quad (3)$$

where ε_i^r and ζ_i^r are smooth mappings defined on $\mathcal{X}_i \times \mathcal{R}_i$. Typically, one of the variables is determined internally by the component dynamics, while the other is imposed via interconnection. Analogously, for control and disturbance interactions, the effort and flow variables are given by,

$$e_i^u = \varepsilon_i^u(x_i, u_i), \quad f_i^u = \zeta_i^u(x_i, u_i), \quad (4)$$

$$e_i^m = \varepsilon_i^m(x_i, m_i), \quad f_i^m = \zeta_i^m(x_i, m_i), \quad (5)$$

with $\varepsilon_i^u, \zeta_i^u$ defined on $\mathcal{X}_i \times \mathcal{U}_i$ and $\varepsilon_i^m, \zeta_i^m$ on $\mathcal{X}_i \times \mathcal{M}_i$.

3.2 Energy space dynamic model

Consider the energy state dynamics of a component Σ_i introduced in (6). Throughout this formulation, we assume that the physical parameters of the component (e.g., resistance, inductance, capacitance) remain constant over time.

$$\dot{E}_i = -\frac{E_i}{\tau_i} + P_i^r + P_i^u + P_i^m, \quad (6a)$$

$$\dot{p}_i = \ddot{E}_i = 4\dot{E}_{t,i} + 2\dot{Q}_{C,i} - \dot{Q}_i^r - \dot{Q}_i^u - \dot{Q}_i^m, \quad (6b)$$

$$\dot{E}_{t,i} = -\frac{E_{t,i}}{\tau_{t,i}} + P_{t,i}^r + P_{t,i}^u + P_{t,i}^m, \quad (6c)$$

where,

- E_i is the stored energy in component Σ_i ,
- p_i is the time derivative of the stored energy,
- $E_{t,i}$ is the stored energy in tangent space,
- $P_i^{(\cdot)}$ are the real power contributions from the corresponding inputs,
- $\dot{Q}_i^{(\cdot)}$ are the corresponding reactive power rates,
- $\dot{Q}_{C,i}$ is the rate of reactive power injected into the capacitor, if present,
- $P_{t,i}^{(\cdot)}$ are the corresponding tangent space power contributions.

Equation (6a) follows directly from energy conservation, expressing the balance between stored energy, dissipation, and external power inputs. Equation (6b) relates the second derivative of stored energy to tangent space energy and generalized reactive power rates; a derivation is provided in [15]. Equation (6c) describes the dynamics of tangent space energy and corresponds to the extended energy formulation introduced in [16]. Its structure mirrors that of (6a), applying the same conservation principle to higher-order quantities using tangent space counterparts.

The third-order energy space model, introduced in [16], enables finer-grained energy-based control synthesis by explicitly modeling $E_{t,i}$ as a state variable. In contrast, earlier second-order models [14,15,25] treated the tangent space energy $E_{t,i}$ as an independent disturbance, an approach that simplifies analysis but is inconsistent with its physical role in the system's energy evolution. The more detailed third-order model introduces a third control interaction, tangent space power, enhancing flexibility, especially in systems with multiple control inputs.

3.3 Interaction Variables

Before we employ the energy space model for distributed control, we define the *port interaction variable* z_i^r , which will be used as the common output in energy space, as specified in (1). Its existence and structural properties are formally established in [26].

Definition 10 (Port Interaction Variable). *The port interaction variable for component Σ_i , denoted z_i^r , is defined as,*

$$z_i^r = \begin{bmatrix} \int_0^t P_i^r(\tau) d\tau \\ \int_0^t \dot{Q}_i^r(\tau) d\tau \\ \int_0^t P_{t,i}^r(\tau) d\tau \end{bmatrix}$$

This variable remains constant, i.e., $\dot{z}_i^r = 0$, when all interconnections with the component are removed.

This variable captures the accumulated energy interactions at the port and is chosen as the common output for distributed control, as its elements obey the generalized Tellegen's theorem [22] and satisfy the feasibility condition in Problem 1. In addition, we define two auxiliary interaction variables: the *control interaction variable* z_i^u and the *exogenous interaction variable* z_i^m , which characterize the effects of control and disturbance inputs, respectively.

Definition 11 (Control Interaction Variable). *The control interaction variable for component Σ_i , denoted z_i^u , is defined as,*

$$z_i^u = \begin{bmatrix} \int_0^t P_i^u(\tau) d\tau \\ \int_0^t \dot{Q}_i^u(\tau) d\tau \\ \int_0^t P_{t,i}^u(\tau) d\tau \end{bmatrix}$$

This variable remains constant when all control inputs are disconnected from the component.

Definition 12 (Exogenous Interaction Variable). *The exogenous interaction variable for component Σ_i , denoted z_i^m , is defined as,*

$$z_i^m = \begin{bmatrix} \int_0^t P_i^m(\tau) d\tau \\ \int_0^t \dot{Q}_i^m(\tau) d\tau \\ \int_0^t P_{t,i}^m(\tau) d\tau \end{bmatrix}$$

This variable remains constant in the absence of external disturbances.

4 Distributed control in energy space

In general, control objectives in an interconnected system can be categorized as *system-level* or *component-level*. System-level control governs the collective behavior of interconnected components to enforce global objectives such as power sharing, minimizing Area Control Error, or damping inter-area oscillations. It determines the power exchanges between components, i.e., the rate of change of the port interaction variables \dot{z}_i^r , which are then allocated as references to each component in a manner that respects their individual capabilities and pro-

notes efficient utilization of controllers. For example, in [16,27], an optimal control problem is formulated to determine the port interaction variables that maximize system-wide efficiency and minimize operational costs. In contrast, component-level control ensures local objectives are met while interacting with the system through the port interaction variable z_i^r prescribed by system-level coordination. This work focuses exclusively on the design of distributed component-level controllers in energy space. We assume that a system-level coordination mechanism already exists, and that the sum of the port interaction variables communicated by neighboring components matches the original system-level allocated reference exactly. These interaction references define local output references used in the control design. The design of system-level coordination mechanism is left for future work.

4.1 Multilayered distributed control architecture

To leverage the benefits of the energy space formulation, we introduce a two-layer modeling structure for each component Σ_i in the interconnected system. The lower layer, or *physical space model*, represents the system using conventional state variables, as described in (1). It captures the nonlinear dynamics as they evolve under control, disturbances, and port inputs. On top of this, we define a higher-level abstraction, the *energy space model*, introduced in Section 3.2. It maps the component's dynamics into a linear form in terms of energy state variables. The linearity enables structured control design, performance guarantees, and a physically intuitive framework for modeling and control. The energy state variable for Σ_i is defined as,

$$x_{z,i} = \begin{bmatrix} E_i \\ p_i \\ E_{t,i} \end{bmatrix}$$

The energy space dynamics are then given by,

$$\text{Initial condition: } x_{z,i}(0) = x_{z,i,0} \quad (7a)$$

Energy space dynamics:

$$\dot{x}_{z,i} = A_{z,i}x_{z,i} + B_{t,i}\dot{Q}_{C,i} + B_{z,i}(\dot{z}_i^r + \dot{z}_i^u + \dot{z}_i^m) \quad (7b)$$

$$\text{Energy space output: } \mathbf{y}_{z,i} = \begin{bmatrix} E_i \\ p_i \end{bmatrix} \quad (7c)$$

Common output:

$$\dot{z}_i^r = \phi_{z,i}(x_{z,i}, \dot{Q}_{C,i}, \dot{z}_i^u, \dot{z}_i^m), \quad z_i^r(0) = z_{i,0}^r \quad (7d)$$

where, The energy state dynamics evolve under the system matrix $A_{z,i}$, with inputs from the rate of change of port, control, and disturbance interaction variables (\dot{z}_i^r , \dot{z}_i^u , \dot{z}_i^m), and an internal variable $\dot{Q}_{C,i}$ capturing reactive power variation due to a capacitor. The system ma-

trix $A_{z,i}$, along with the input matrices $B_{z,i}$ and $B_{t,i}$ are given by,

$$A_{z,i} = \begin{bmatrix} -\frac{1}{\tau_i} & 0 & 0 \\ 0 & 0 & 4 \\ 0 & 0 & -\frac{1}{\tau_{t,i}} \end{bmatrix}, \quad B_{t,i} = 2, \quad B_{z,i} = 1$$

$\mathbf{y}_{z,i}$ denotes the local energy space output of interest for which the energy space control is designed. The port interaction variable z_i^r is chosen as the common output, as it is physically shared with neighboring components. Moreover, z_i^r satisfies structural properties from the generalized Tellegen's theorem, serving as a consistency condition for interconnection feasibility.

In this work, we consider each component Σ_i to have a single physical output y_i and a single physical control input u_i . The extension to multiple outputs and multiple control inputs will be addressed in future work. Given the single degree of freedom in the control input, we introduce a higher-layer input $u_{z,i} \in \mathbb{R}$, termed the *primary control input* in the energy space. All control interactions are realized as functions of $u_{z,i}$ and the physical state x_i via a technology-dependent mapping,

$$\dot{z}_i^u = U_i(u_{z,i}, x_i)$$

Similarly, since there is a single physical output y_i , the corresponding energy space output is defined as in (7c). Although $\mathbf{y}_{z,i}$ is two-dimensional, it encodes only one degree of freedom due to the constraint $p_i = \dot{E}_i$. The output reference is similarly lifted to energy space,

$$\mathbf{y}_{z,i}^{ref} = \begin{bmatrix} E_i^{ref} \\ p_i^{ref} \end{bmatrix} \quad (8)$$

To ensure that tracking $\mathbf{y}_{z,i}^{ref}$ implies tracking y_i^{ref} , we assume the physical output reference can be lifted via a smooth, invertible map,

$$\mathbf{y}_{z,i}^{ref} = \Phi_{\dot{z}_j^r}(y_i^{ref})$$

where the mapping $\Phi_{\dot{z}_j^r}$ may depend on the interactions \dot{z}_j^r communicated by neighboring components. We now state the assumptions used in this work.

Assumption 1. The time constant τ_i and the tangent space time constant $\tau_{t,i}$ are strictly positive for all time.

Assumption 2. Given the port input $r_i(t)$, control input $u_i(t)$, and exogenous input $m_i(t)$, there exists a non-empty set of state trajectories $\mathcal{X}_{eq,i}(t) \subseteq \mathcal{X}_i$ such that,

$$y_i(t) = y_i^{ref}(t) \quad \forall \quad x_i(t) \in \mathcal{X}_{eq,i}(t)$$

where $y_i = f_{y,i}(x_i, u_i, r_i, m_i)$ as defined in (1).

Assumption 3. The rate of change of the control interaction is given by a smooth map $U_i : \mathbb{R} \times \mathcal{X}_i \rightarrow \mathbb{R}^3$,

$$\dot{z}_i^u = U_i(u_{z,i}, x_i) \quad (9)$$

where $u_{z,i} \in \mathbb{R}$ is the primary control input in energy space, and $x_i \in \mathcal{X}_i$ is the component's physical state.

Assumption 4. There exists a smooth, uniquely defined mapping $d_i : \mathbb{R} \times \mathcal{X}_i \rightarrow \mathcal{U}_i$ from the energy space control input to the physical control input,

$$u_i = d_i^u(u_{z,i}, x_i) \quad (10)$$

This ensures that control inputs designed in energy space are physically implementable.

Assumption 5. There exists a smooth, invertible mapping $\Phi_{z_j^r} : \mathbb{R} \rightarrow \mathbb{R}^2$ from the physical output reference to the corresponding energy space reference,

$$\mathbf{y}_{z,i}^{ref} = \Phi_{z_j^r}(y_i^{ref}) \quad (11)$$

where $\Phi_{z_j^r}$ may depend on the rate of port interactions \dot{z}_j^r communicated by neighboring components.

For each component Σ_i , the multilayered distributed control architecture operates by measuring the physical state, lifting it to energy space, designs an energy space control input using local and neighbor information, and mapping it back to the physical space for implementation, as shown in Figure 2.

- (1) **State measurement (lower layer):** Each component Σ_i measures its physical state x_i .
- (2) **Lifting to energy space:** Each component computes its energy state $(E_i, p_i, E_{t,i})$ and internal variable $\dot{Q}_{C,i}$, if a capacitor is present.
- (3) **Energy space control design:** The primary control input $u_{z,i}$ is computed using available system information such as,
 - energy state $x_{z,i}$ and internal variable $\dot{Q}_{C,i}$,
 - rate of port interactions \dot{z}_j^r received from neighboring components Σ_j ,
 - energy space output reference $\mathbf{y}_{z,i}^{ref}$ from (11).
The primary control input $u_{z,i}$ is then determined as a smooth function of the local energy state, internal variable, neighbor interactions, and output reference,

$$u_{z,i} = c_{z,i}(x_{z,i}, \dot{Q}_{C,i}, \dot{z}_j^r, \mathbf{y}_{z,i}^{ref}), \quad j \in \mathcal{C}_i$$

- (4) **Mapping to physical control input:** The primary control input $u_{z,i}$ is mapped to the physical control input u_i via (10) and implemented.

At the next time step, after implementing u_i updating its state x_i , component Σ_i computes its rate of change of

port interaction \dot{z}_i^r using (7d), using either either state measurements or an observer. This value is then shared with neighboring components for the next distributed control iteration.

Remark 1. Although each component Σ_i can compute its own port interaction \dot{z}_i^r locally using updated state information or an observer, communication with neighbors is essential. In practice, neighboring components may not perfectly realize their system-level allocated references, requiring Σ_i (or others) to adjust \dot{z}_i^r to satisfy overall demand. Two-way communication thus enables detection and correction of deviations, facilitating coordinated control across the network. In this work, we assume that the sum of the rate of change of port interactions received from neighboring components, $\sum_{j \in \mathcal{C}_i} \dot{z}_j^r$, matches the original local system-level reference $\dot{z}_i^{r,ref}$ exactly.

4.2 Distributed control problem posing in energy space

Building on the general distributed control framework in Problem 1, we now pose the corresponding control problem in energy space.

Problem 2 (Distributed control problem formulation in energy space). Given an interconnected system consisting of a set \mathcal{N} of components, the objective is to design a smooth distributed feedback control law of the form,

$$u_{z,i} = c_{z,i}(x_{z,i}, \dot{Q}_{C,i}, \dot{z}_j^r, \mathbf{y}_{z,i}^{ref}), \quad j \in \mathcal{C}_i, \quad \forall i \in \mathcal{N} \quad (12)$$

which depends on the local energy state $x_{z,i}$, internal variable $\dot{Q}_{C,i}$, minimal information \dot{z}_j^r communicated by neighboring components Σ_j , and the energy space output reference $\mathbf{y}_{z,i}^{ref}$, such that the following conditions are satisfied:

- (1) **Feasibility constraint:** The rate of change of port interaction variables must satisfy,

$$\dot{z}_i^r = - \sum_{j \in \mathcal{C}_i} \dot{z}_j^r, \quad \forall i \in \mathcal{N} \quad (13)$$

This condition is inherently satisfied via generalized Tellegen's theorem due to the choice of the port interaction variable as the common output.

- (2) **Control objective:** The energy space output $\mathbf{y}_{z,i}$ must track a consistent reference $\mathbf{y}_{z,i}^{ref}$ given by the smooth map $\Phi_{z_j^r}$ as defined in (11),

$$\mathbf{y}_{z,i}(t) \rightarrow \mathbf{y}_{z,i}^{ref}(t) \quad \text{as } t \rightarrow \infty, \quad \forall i \in \mathcal{N}$$

5 Energy-based component-level control design

For the distributed energy space control problem posed in Problem 2, a generalized higher-level control design methodology is introduced in this section. We select

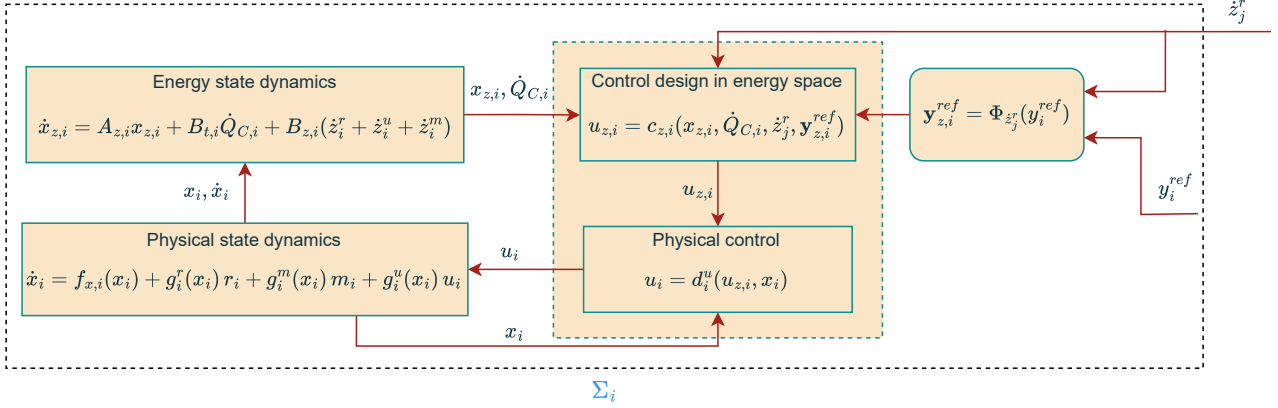


Fig. 2. Multilayered distributed control architecture for a component Σ_i

$u_{z,i} := \dot{Q}_i^u$ as the primary higher level control input. Other energy space control interactions (e.g., P_i^u , $P_{t,i}^u$) are determined by \dot{Q}_i^u and the component's technology via (9). The primary control input $u_{z,i}$, as defined in (12), is a function of the available system information, namely the energy state variables, the internal variable, the communicated neighbor interactions, and the energy space output reference. This formulation assumes full physical state space observability, meaning that the energy state variables $x_{z,i}$ and the internal variable $\dot{Q}_{C,i}$ are known, as they are functions of the underlying physical state variables of the component. Given communicated neighbor interactions \dot{z}_j^r , each component computes its local interaction variable \dot{z}_i^r according to the generalized Tellegen's theorem, as given in (13). Any deviations or estimation errors in the communicated port interaction variables are absorbed into the exogenous disturbance term \dot{z}_i^m , without affecting the structural feasibility conditions. Finally, the energy space output reference $\mathbf{y}_{z,i}^{ref}$ is determined by lifting the physical output reference y_i^{ref} via the smooth mapping in (5).

Now, consider the proposed energy space output variable and its reference in the equations (7c) and (8). Taking the time derivative of their difference, and substituting the energy space dynamics from (6a) and (6b), we obtain the following input-output relation for the evolution of the energy space tracking error,

$$\dot{\mathbf{y}}_{z,i} - \dot{\mathbf{y}}_{z,i}^{ref} = \begin{bmatrix} p_i - p_i^{ref} \\ 4E_{t,i} + 2\dot{Q}_{C,i} - \dot{Q}_i^r - \dot{Q}_i^u - \dot{Q}_i^m - \dot{p}_i^{ref} \end{bmatrix} \quad (14)$$

Next, we propose two distinct energy-based control design methods that leverage equation (14), each leading to qualitatively different closed-loop behaviors and robustness properties.

5.1 Energy-based feedback linearizing control (FBLC)

Feedback linearizing control (FBLC) is a nonlinear control technique [28] that cancels system nonlinearities by applying an exact transformation through the control input. In order to ensure $\mathbf{y}_{z,i}$ tracks $\mathbf{y}_{z,i}^{ref}$, we propose the following energy-based FBLC design,

$$u_{z,i}^{fblc} = 4E_{t,i} + 2\dot{Q}_{C,i} + \sum_{j \in \mathcal{C}_i} \dot{Q}_j^r + K_1(E_i - E_i^{ref}) + K_2(p_i - p_i^{ref}) - \dot{p}_i^{ref} \quad (15)$$

where, $K_1, K_2 > 0$ are constant gains. Clearly, $u_{z,i}^{fblc}$ depends only on the available system information, as defined in (12): the energy state variables ($E_i, p_i, E_{t,i}$), internal variable $\dot{Q}_{C,i}$, neighbor interactions \dot{Q}_j^r , and energy space output references (E_i^{ref}, p_i^{ref}).

Substituting (15) into (14) and applying (13), the closed-loop system becomes,

$$\begin{aligned} \dot{\mathbf{y}}_{z,i} - \dot{\mathbf{y}}_{z,i}^{ref} &= \begin{bmatrix} p_i - p_i^{ref} \\ -K_1(E_i - E_i^{ref}) - K_2(p_i - p_i^{ref}) - \dot{Q}_i^m \end{bmatrix} \\ &= \begin{bmatrix} y_{z,i}^2 - y_{z,i}^{2,ref} \\ -K_1(y_{z,i}^1 - y_{z,i}^{1,ref}) - K_2(y_{z,i}^2 - y_{z,i}^{2,ref}) - \dot{Q}_i^m \end{bmatrix} \end{aligned} \quad (16)$$

where $y_{z,i}^1 = E_i$ and $y_{z,i}^2 = p_i$. Based on the closed-loop energy space output dynamics in (16), we now establish sufficient conditions for asymptotic convergence of $\mathbf{y}_{z,i} \rightarrow \mathbf{y}_{z,i}^{ref}$.

Theorem 5.1 (Performance with energy-based FBLC). *Consider the virtual control $u_{z,i} = \dot{Q}_i^u$ in (15). Under the assumptions stated earlier, the closed-loop energy space*

output dynamics (16) are asymptotically stable if,

$$|\dot{Q}_i^m| \leq K_2 |p_i - p_i^{ref}| \quad (17)$$

Proof. Consider the candidate Lyapunov function,

$$V_i^{fblc}(\mathbf{y}_{z,i} - \mathbf{y}_{z,i}^{ref}) = \frac{1}{2} \left(K_1 (y_{z,i}^1 - y_{z,i}^{1,ref})^2 + (y_{z,i}^2 - y_{z,i}^{2,ref})^2 \right)$$

V_i^{fblc} is a valid Lyapunov function since $V_i^{fblc} = 0$ if and only if $\mathbf{y}_{z,i} - \mathbf{y}_{z,i}^{ref} = \mathbf{0}$, and $V_i^{fblc} > 0$ otherwise. It is thus positive definite and radially unbounded with respect to the tracking error. Taking its time derivative and substituting the closed-loop dynamics (16) yields,

$$\begin{aligned} \dot{V}_i^{fblc} &= K_1 \left(y_{z,i}^1 - y_{z,i}^{1,ref} \right) \left(y_{z,i}^2 - y_{z,i}^{2,ref} \right) \\ &\quad + \left(y_{z,i}^2 - y_{z,i}^{2,ref} \right) \left(-K_1 (y_{z,i}^1 - y_{z,i}^{1,ref}) \right. \\ &\quad \left. - K_2 (y_{z,i}^2 - y_{z,i}^{2,ref}) - \dot{Q}_i^m \right) \\ &= -K_2 \left(y_{z,i}^2 - y_{z,i}^{2,ref} \right)^2 - \dot{Q}_i^m \left(y_{z,i}^2 - y_{z,i}^{2,ref} \right) \end{aligned} \quad (18)$$

Applying the condition (17), we obtain,

$$\dot{V}_i^{fblc} \leq 0$$

Thus, \dot{V}_i^{fblc} is negative semi-definite. This proves Lyapunov stability; to prove asymptotic stability, we use LaSalle's invariance principle. Equation (18) indicates that, for arbitrary \dot{Q}_i^m values, the largest invariant set of points $\mathbf{y}_{z,i} \in \mathbb{R}$ that satisfies $\dot{V}_i^{fblc} = 0$ is the equilibrium $\mathbf{y}_{z,i} = \mathbf{y}_{z,i}^{ref}$. This is because if $y_{z,i}^1 \neq y_{z,i}^{1,ref}$ or $y_{z,i}^2 \neq y_{z,i}^{2,ref}$ then by equation (16) $\dot{y}_{z,i}^2 \neq \dot{y}_{z,i}^{2,ref}$, violating invariance. Hence, the closed-loop energy space output dynamics are asymptotically stable. \square

Condition (17) implies that the deviation $p_i - p_i^{ref}$ is lower-bounded by the magnitude of the of the exogenous disturbance \dot{Q}_i^m . Hence, p_i cannot fully converge to p_i^{ref} and instead oscillates with a minimum amplitude of $|\dot{Q}_i^m|/K_2$. Reducing this disturbance is therefore key to improving FBLC stability and tracking performance.

5.2 Energy-based sliding mode control (SMC)

Sliding mode control (SMC) is a robust nonlinear control technique [28] that drives system trajectories onto a prescribed sliding surface in finite time and maintains them there, ensuring robustness to model uncertainties

and disturbances. For the energy-based SMC design, consider the sliding surface,

$$\sigma_i := p_i - p_i^{ref} + M_1(E_i - E_i^{ref}) = 0$$

On this surface, asymptotic convergence of $\mathbf{y}_{z,i} \rightarrow \mathbf{y}_{z,i}^{ref}$ is ensured. We propose the following SMC control design in energy space,

$$\begin{aligned} u_{z,i}^{smc} &= 4E_{t,i} + 2\dot{Q}_{C_i} + \sum_{j \in \mathcal{C}_i} \dot{Q}_j^r + M_1(p_i - p_i^{ref}) \\ &\quad + M_o \text{sign}(\sigma_i) \end{aligned} \quad (19)$$

where $M_o, M_1 > 0$ are gain constants. Similar, to the energy-based FBLC, $u_{z,i}^{smc}$ is constructed only from the available system information, as defined in (12).

Substituting (19) into (14) and applying (13), the closed-loop dynamics become,

$$\dot{\mathbf{y}}_{z,i} - \dot{\mathbf{y}}_{z,i}^{ref} = \begin{bmatrix} p_i - p_i^{ref} \\ -M_o \text{sign}(\sigma_i) - M_1(p_i - p_i^{ref}) - \dot{Q}_i^m \end{bmatrix} \quad (20)$$

From the closed-loop energy space output dynamics (20), we now establish sufficient conditions for finite-time convergence to the sliding surface and asymptotic convergence of $\mathbf{y}_{z,i} \rightarrow \mathbf{y}_{z,i}^{ref}$.

Theorem 5.2 (Performance with energy-based SMC). *Consider the virtual control $u_{z,i} = \dot{Q}_i^u$ in (19). Under the assumptions stated earlier, the closed-loop energy space output dynamics (20) achieve finite reaching time to the sliding surface $\sigma_i = 0$ within a time t_r upper bounded by,*

$$t_r \leq \frac{|\sigma_i(0)|}{M_o - \bar{M}}$$

provided that,

$$|\dot{Q}_i^m| \leq \bar{M} < M_o \quad (21)$$

where $\sigma_i := p_i - p_i^{ref} + M_1(E_i - E_i^{ref})$ and $|\sigma_i(0)|$ is the initial distance to the sliding surface. Furthermore, once on the sliding surface, the closed-loop energy space output dynamics are asymptotically stable.

Proof. Consider the candidate Lyapunov function,

$$V_i^{smc}(\sigma_i) = \frac{1}{2} \sigma_i^2$$

Taking its time derivative and plugging in the expres-

sions from the closed-loop dynamics (20) yields,

$$\begin{aligned}\dot{V}_i^{smc} &= \sigma_i \dot{\sigma}_i \\ &= \sigma_i \left(\dot{p}_i - \dot{p}_i^{ref} + M_1(p_i - p_i^{ref}) \right) \\ &= \sigma_i \left(-M_o \text{sign}(\sigma_i) - \dot{Q}_i^m \right) \\ &= -M_o |\sigma_i| - \dot{Q}_i^m \sigma_i\end{aligned}$$

Applying the condition (21), we obtain,

$$\dot{V}_i^{smc} \leq -(M_o - \bar{M})|\sigma_i| < 0 \quad (22)$$

showing that \dot{V}_i^{smc} is negative definite. Integrating (22), we find,

$$\begin{aligned}\dot{V}_i^{smc} &\leq -(M_o - \bar{M})\sqrt{2V_i^{smc}} \\ \sqrt{2V_i^{smc}(t_r)} - \sqrt{2V_i^{smc}(0)} &\leq -(M_o - \bar{M})t_r \\ |\sigma_i(t_r)| - |\sigma_i(0)| &\leq -(M_o - \bar{M})t_r\end{aligned}$$

Setting $\sigma_i(t_r) = 0$ yields,

$$t_r \leq \frac{|\sigma_i(0)|}{M_o - \bar{M}}$$

Once the sliding surface $\sigma_i = 0$ is reached, the system evolves according to

$$p_i = -M_1(E_i - E_i^{ref}) + p_i^{ref},$$

ensuring asymptotic convergence of $\mathbf{y}_{z,i} \rightarrow \mathbf{y}_{z,i}^{ref}$. \square

The condition (21) is less conservative than the energy-based FBLC condition (17), as it only requires a constant bound on the disturbance $|\dot{Q}_i^m|$, ensuring $p_i \rightarrow p_i^{ref}$ if $|\dot{Q}_i^m| \leq \bar{M}$. Additionally, the energy-based SMC ensures finite reaching time, unlike the asymptotic stability result of energy-based FBLC, making it well-suited for scenarios requiring timely tracking of references. While SMC is inherently robust to model uncertainties and external disturbances, it may introduce chattering due to high-frequency switching, often requiring smoothing techniques for practical implementation.

6 Examples

This section evaluates the proposed energy-based distributed control methods through two examples. The first involves an inverter-controlled voltage source in an RLC circuit supplying constant and time-varying loads, with voltage stability and regulation as the objective. The second examines a synchronous generator supplying power to a smooth step load, where the goal is to stabilize

and regulate frequency. In both cases, the energy-based FBLC and SMC controllers are compared against conventional benchmark controllers to demonstrate their performance.

6.1 Voltage regulation in an RLC circuit

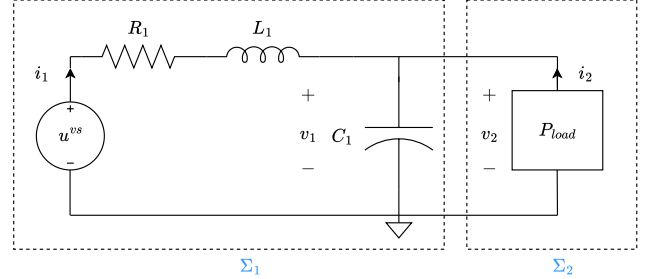


Fig. 3. RLC circuit with an inverter-controlled voltage source u^{vs} (Σ_1) supplying power to a black-box with unknown internal dynamics (Σ_2)

Figure 3 shows an RLC circuit with an inverter-controlled voltage source u^{vs} supplying power to a load with specified power demand P_{load} . The control objective is to stabilize and regulate the terminal voltage v_1 to 80 V. The system is modeled as two interacting sub-systems: the source Σ_1 and the load Σ_2 , consistent with the general structure in Figure 1. The physical state and control variables of Σ_1 are,

$$x_1 = \begin{bmatrix} i_1 \\ v_1 \end{bmatrix}, \quad u_1 = u^{vs}$$

where i_1 is the current flowing through the inductor L_1 , and v_1 is the voltage across the capacitor C_1 . R_1 represents the resistance in series with the inductor. The lower level physical state space model for Σ_1 is given by,

$$\begin{aligned}\frac{d}{dt} \underbrace{\begin{bmatrix} i_1 \\ v_1 \end{bmatrix}}_{x_1} &= \underbrace{\begin{bmatrix} -\frac{R_1}{L_1} & -\frac{1}{L_1} \\ \frac{1}{C_1} & 0 \end{bmatrix}}_{f_{x,1}(x_1)} \underbrace{\begin{bmatrix} i_1 \\ v_1 \end{bmatrix}}_{x_1} + \underbrace{\begin{bmatrix} \frac{1}{L_1} \\ 0 \end{bmatrix}}_{g_1^u(x_1)} \underbrace{u^{vs}}_{u_1} \\ &+ \underbrace{\begin{bmatrix} 0 \\ -\frac{1}{C_1 v_1} \end{bmatrix}}_{g_1^r(x_1)} \underbrace{P_{load}}_{r_1}\end{aligned}$$

To design the energy-based distributed controller for Σ_1 , we define the relevant effort-flow pairs using Equations (3) and (4),

$$\left. \begin{aligned} e_1^u &= u_1, & f_1^u &= i_1 \\ e_1^C &= v_1, & f_1^C &= C_1 \dot{v}_1 \end{aligned} \right\} \quad (\text{for } \Sigma_1)$$

$$e_2^r = v_2, \quad f_2^r = \frac{P_{load}}{v_2} \quad (\text{for } \Sigma_2)$$

Subsystem Σ_1 has access to its internal states, as well as the port interaction variable \dot{z}_2^r received from Σ_2 . Subsystem Σ_2 computes $\dot{z}_2^r = \begin{bmatrix} P_2^r & \dot{Q}_2^r & P_{t,2}^r \end{bmatrix}^\top$ as,

$$\begin{aligned} P_2^r &= P_{load} \\ \dot{Q}_2^r &= v_2 \frac{d}{dt} \left(\frac{P_{load}}{v_2} \right) - \left(\frac{P_{load}}{v_2} \right) \frac{dv_2}{dt} \\ &= \frac{dP_{load}}{dt} - 2 \frac{P_{load}}{v_2} \frac{dv_2}{dt} \\ P_{t,2}^r &= \frac{dv_2}{dt} \cdot \frac{d}{dt} \left(\frac{P_{load}}{v_2} \right) \end{aligned}$$

While P_{load} is externally specified, the quantities \dot{Q}_2^r and $P_{t,2}^r$ are left unspecified and act as free variables. These quantities dynamically adjust to ensure that load Σ_2 consumes the desired active power. By the conservation law at the interconnection (13), we thus have,

$$\dot{z}_1^r = -\dot{z}_2^r$$

Subsystem Σ_1 computes its energy space vector, $x_{z,1} = \begin{bmatrix} E_1 & p_1 & E_{t,1} \end{bmatrix}^\top$, along with its internal variable $Q_{C,1}$, using local state measurements,

$$\begin{aligned} E_1 &= \frac{1}{2} L_1 i_1^2 + \frac{1}{2} C_1 v_1^2 \\ p_1 &= L_1 i_1 \frac{di_1}{dt} + C_1 v_1 \frac{dv_1}{dt} \\ E_{t,1} &= \frac{1}{2} L_1 \left(\frac{di_1}{dt} \right)^2 + \frac{1}{2} C_1 \left(\frac{dv_1}{dt} \right)^2 \\ \dot{Q}_{C,1} &= C_1 v_1 \frac{d^2 v_1}{dt^2} - C_1 \left(\frac{d^2 v_1}{dt^2} \right)^2 \end{aligned}$$

The output of interest is selected as $y_1 = v_1$, i.e., the port voltage, which is to be stabilized and regulated to a reference value of $y_1^{ref} = 80$ V. The corresponding higher level energy space output references are thus,

$$\mathbf{y}_{z,1}^{ref} = \begin{bmatrix} E_1^{ref} \\ p_1^{ref} \end{bmatrix} = \begin{bmatrix} \frac{1}{2} L_1 \left(\frac{P_{load}}{y_1^{ref}} \right)^2 \\ L_1 \frac{P_{load}}{y_1^{ref2}} \dot{P}_{load} \end{bmatrix}$$

The higher level primary control input $u_{z,1}$ is mapped to the lower level physical control input u_1 via the technology-specific transformation in (10). For the RLC subsystem, the mapping function $d_1^u(u_{z,1}, x_1)$ is characterized by the differential relation,

$$\frac{du_1}{dt} = \frac{u_1}{i_1} \frac{di_1}{dt} - \frac{u_{z,1}}{i_1}$$

While this may not yield an explicit closed-form ex-

pression for u_1 , it provides a realizable dynamic relation based on the history and current value of u_1 , local state variables x_1 , and the higher level primary control input $u_{z,1}$. The dynamic control law is initialized with $u_1(0) = 79$ V, enabling closed-loop evolution of $u_1(t)$. For all simulations and analysis, we use the following parameter values,

$$R_1 = 100 \text{ m}\Omega, \quad L_1 = 1.12 \text{ mH}, \quad C_1 = 6.8 \text{ mF}$$

with initial conditions,

$$i_1(0) = 12.8 \text{ A}, \quad v_1(0) = 79 \text{ V}$$

6.1.1 Constant power load

Consider a constant power load $P_{load} = 1$ kW. First, we create a benchmark test using a conventional proportional control design given by,

$$u_p^{vs} = u_{ref}^{vs} - K_i \left(i_1 - \frac{P_{load}}{y_1^{ref}} \right) - K_v (v_1 - y_1^{ref}) \quad (23)$$

where u_{ref}^{vs} is the reference input applied at equilibrium,

$$u_{ref}^{vs} = y_1^{ref} + R_1 \frac{P_{load}}{y_1^{ref}}$$

The proportional control gains are chosen as,

$$K_i = 5, \quad K_v = 0.5 \quad (24)$$

A limitation of proportional control for general nonlinear systems is that the gains K_i and K_v in (24) are typically selected empirically through experimental tuning. The resulting benchmark control input u_p^{vs} yields a stable response, as shown by the blue trajectories in Figure 4.

For the energy-based FBLC and SMC methods, the higher level control input $u_{z,1}$ is derived using (15) and (19), respectively. Assuming no exogenous disturbances, i.e., $\dot{z}_1^m = 0$, the energy-based FBLC gains are set as,

$$K_1 = K_2 = 10, \quad (25)$$

and the energy-based SMC gains as,

$$M_o = 5.4, \quad M_1 = 2.9 \quad (26)$$

The resulting system responses with energy-based FBLC and SMC are shown in Figure 4, represented by the red and green trajectories, respectively. The gain values chosen in (25) and (26) ensure stable performance with tolerable transient overshoots. These gains can be tuned

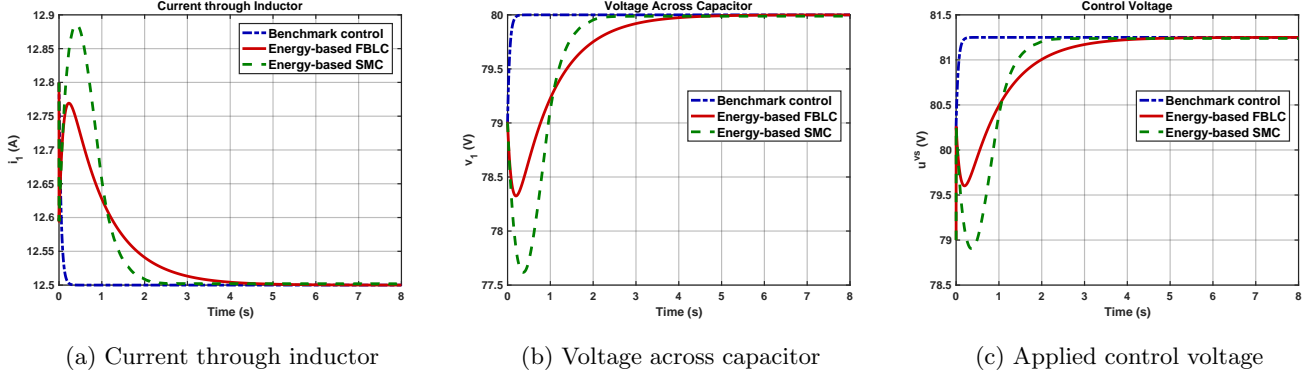


Fig. 4. System response of the RLC circuit under proportional benchmark control (23), energy-based FBLC, and energy-based SMC for a constant power load of 1 kW, with the objective of stabilizing and regulating the terminal voltage v_1 to 80 V

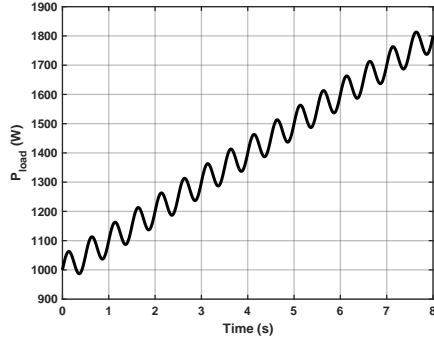


Fig. 5. Time-varying load profile with non-zero mean power

further based on the desired transient response characteristics. Notably, the energy-based SMC demonstrates a finite reaching time whereas the energy-based FBLC exhibits smooth exponential convergence.

6.1.2 Time-varying power load

Consider the time-varying load profile to be served as shown in Figure 5. Conventional constant-gain proportional controllers fail to regulate voltage under such time-varying power demands. As an alternative, we consider a nonlinear benchmark control proposed in [29] which is based on the Brayton-Moser potential function formulation. The control law is as follows,

$$u_{bm}^{vs} = y_1^{ref} + R_1 i_1 - L_1 \left(\frac{\Pi}{v_1^2} + N_3 \right) \frac{dv_1}{dt} - \left(N_1 (v_1 - y_1^{ref}) + N_2 \frac{dv_1}{dt} \right) \quad (27)$$

This control includes an adaptive gain term $\frac{\Pi}{v_1^2} + N_3$, where Π is the upper bound on the load power values being served. It has been shown in [29] that the control law in (27) results in stable performance for all $y_1^{ref} > 0$

and $P_{load} \leq \Pi$. The controller gains are chosen as,

$$N_1 = 8, \quad N_2 = 1, \quad N_3 = 2, \quad \Pi = 3 \cdot 10^3 \quad (28)$$

For the energy-based FBLC and SMC methods, the same gain values are used as given in (25) and (26). Figure 6 compares trajectories under the nonlinear benchmark control u_{bm}^{vs} , shown in blue, with energy-based FBLC and SMC results, shown in red and green, respectively. All controllers successfully stabilize and regulate the terminal voltage v_1 to 80 V; however, their transient behaviors differ considerably.

The benchmark controller shows significant overshoot with the gains in (28), while achieving a settling time comparable to the energy-based controllers. A smoother response could be obtained by further tuning the gains, though this would likely come at the expense of an increased settling time. Additionally, the gain parameter Π is constrained by the maximum load power to be served, limiting the flexibility of gain tuning for a desired system response. In contrast, the energy-based controllers give smoother transients and lower rates of change in the control input u^{vs} , as shown in Figure 6c, leading to lower actuator wear and tear. Overall, the energy-based FBLC and SMC controllers demonstrate improved transient behavior and robustness under time-varying load conditions, with energy-based SMC offering faster convergence due to its finite-time reaching property.

6.2 Frequency regulation in a synchronous generator

Figure 7 depicts a synchronous generator supplying power to a load with specified power demand P_{load} . The control objective is to stabilize and regulate the generator frequency ω_1 to 60 Hz or 377 rad/s under load variations. Figure 8 shows a zoomed-in block diagram of the generator's internal dynamics including the rotor, turbine and governor control system. The physical state

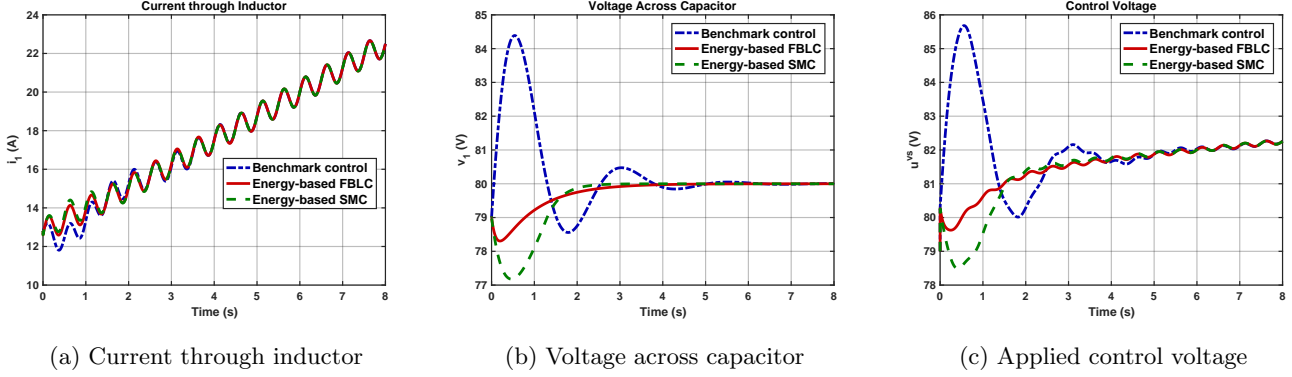


Fig. 6. System response of the RLC circuit under nonlinear benchmark control (27), energy-based FBLC, and energy-based SMC for a time-varying power load, with the objective of stabilizing and regulating the terminal voltage v_1 to 80 V

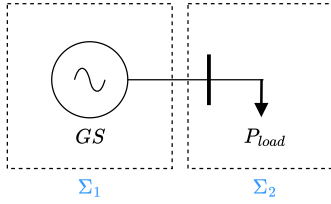


Fig. 7. Synchronous generator with controllable turbine valve position a_1 (Σ_1) supplying power to a black-box load with unknown internal dynamics (Σ_2)

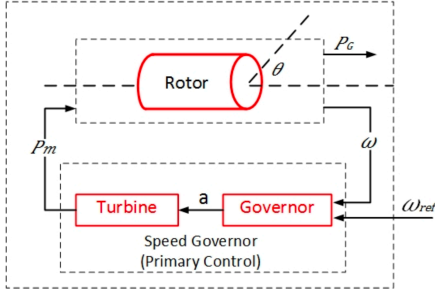


Fig. 8. Block diagram of the generator-turbine-governor system

and control variables of subsystem Σ_1 are,

$$x_1 = \begin{bmatrix} \omega_1 \\ P_{m,1} \end{bmatrix}, \quad u_1 = a_1$$

where ω_1 is the angular speed of the rotor (i.e., the generator frequency), $P_{m,1}$ is the mechanical power output of the turbine and a_1 is the governor-controlled valve position that modulates the steam flow into the turbine. For simplicity, we use the classical swing equation to model the rotor dynamics and an IEEE Type-1 linear model to represent the turbine. Since we are focusing on an isolated case of frequency control, voltage dynamics are not

considered in this model.

$$\begin{aligned} \frac{d}{dt} \underbrace{\begin{bmatrix} \omega_1 \\ P_{m,1} \end{bmatrix}}_{x_1} &= \underbrace{\begin{bmatrix} -\frac{D_1}{J_1} & \frac{1}{J_1\omega_1} \\ 0 & -\frac{1}{T_t} \end{bmatrix}}_{f_{x,1}(x_1)} \underbrace{\begin{bmatrix} \omega_1 \\ P_{m,1} \end{bmatrix}}_{x_1} + \underbrace{\begin{bmatrix} 0 \\ \frac{K_t}{T_t} \end{bmatrix}}_{g_1^u(x_1)} \underbrace{a_1}_{u_1} \\ &+ \underbrace{\begin{bmatrix} -\frac{1}{J_1\omega_1} \\ 0 \end{bmatrix}}_{g_1^r(x_1)} \underbrace{P_{load}}_{r_1} \end{aligned}$$

where J_1 is the moment of inertia, D_1 is the damping coefficient, T_t is the turbine time constant, and K_t is the turbine gain. To design the energy-based control for Σ_1 , we identify the relevant effort and flow variables using Equations (4) and (3),

$$\begin{aligned} e_1^u &= \frac{P_{m,1}}{\omega_1}, & f_1^u &= \omega_1 & (\text{for } \Sigma_1) \\ e_2^r &= \frac{P_{load}}{\omega_2}, & f_2^r &= \omega_2 & (\text{for } \Sigma_2) \end{aligned}$$

where $\omega_2 (= \omega_1)$ is the electrical frequency at subsystem Σ_2 . Subsystem Σ_1 has access to its internal states, as well as the port interaction variable \dot{z}_2^r received from Σ_2 . Subsystem Σ_2 computes \dot{z}_2^r as,

$$\begin{aligned} P_2^r &= P_{load} \\ \dot{Q}_2^r &= \frac{P_{load}}{\omega_2} \frac{d\omega_2}{dt} - \omega_2 \frac{d}{dt} \left(\frac{P_{load}}{\omega_2} \right) \\ &= -\frac{dP_{load}}{dt} + 2 \frac{P_{load}}{\omega_2} \frac{d\omega_2}{dt} \\ P_{t,2}^r &= \frac{d}{dt} \left(\frac{P_{load}}{\omega_2} \cdot \frac{d\omega_2}{dt} \right) \end{aligned}$$

As in the previous example, \dot{Q}_2^r and $P_{t,2}^r$ are unspecified and act as free variables. Using local state measure-

ments, subsystem Σ_1 computes $x_{z,1}$ as,

$$\begin{aligned} E_1 &= \frac{1}{2} J_1 \omega_1^2 \\ p_1 &= J_1 \omega_1 \frac{d\omega_1}{dt} \\ E_{t,1} &= \frac{1}{2} J_1 \left(\frac{d\omega_1}{dt} \right)^2 \end{aligned}$$

Since the dominant inertia in the system arises from the rotor, it is reasonable to neglect the turbine's inertia. As the system lacks capacitive components, $\dot{Q}_{C,1} = 0$. The output of interest is selected as $y_1 = \omega_1$, which is to be stabilized and regulated to a reference value of $y_1^{ref} = 377$ rad/s. The higher level energy space output references are thus,

$$\mathbf{y}_{z,1}^{ref} = \begin{bmatrix} E_1^{ref} \\ p_1^{ref} \end{bmatrix} = \begin{bmatrix} \frac{1}{2} J_1 y_1^{ref^2} \\ 0 \end{bmatrix}$$

For the synchronous generator subsystem considered here, the mapping function $d_1^u(u_{z,1}, x_1)$ in (10) is explicitly characterized by the following relation,

$$u_1 = d_1^u(u_{z,i}, x_1) := \frac{T_t \left(2\dot{\omega}_1 \frac{P_{m,1}}{\omega_1} - u_{z,1} \right) + P_{m,1}}{K_t}$$

The simulation uses the following parameter values,

$$\begin{aligned} J_1 &= 10 \text{ kg} \cdot \text{m}^2, & D_1 &= 0.01 \text{ N} \cdot \text{m} \cdot \text{s} / \text{rad}, \\ T_t &= 0.5 \text{ s}, & K_t &= 1000 \text{ W} / \text{cm} \end{aligned}$$

with initial conditions,

$$\omega_1(0) = 373.23 \text{ rad/s}, \quad P_{m,1}(0) = 1 \text{ kW}$$

6.2.1 Smooth step power load

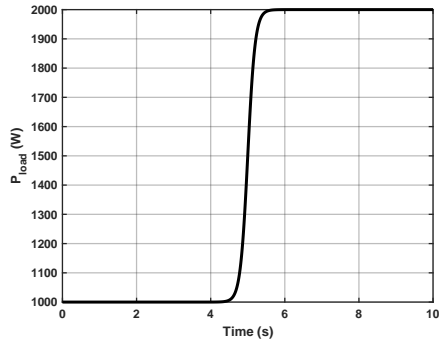


Fig. 9. Smooth step (sigmoid) load profile

Consider a smooth step change in power demand, implemented using a sigmoid function as shown in Figure 9.

As a benchmark, we simulate the conventional primary frequency control scheme commonly used in practice,

$$\dot{a}_1 = -\frac{a_1}{T_g} - \frac{1}{T_g} \frac{\omega_1 - y_1^{ref}}{r} \quad (29)$$

where T_g is the governor time constant and r is the droop coefficient. For this example, the droop gain is chosen as $r = 0.2$. A major disadvantage of the conventional governor controller is the steady-state frequency error it introduces, proportional to the load change, as seen in the blue trajectory of Figure 10a. This necessitates secondary frequency control, typically acting on a slower timescale to restore frequency to its nominal value.

For the energy-based FBLC and SMC, the higher level control input $u_{z,1}$ is computed using (15) and (19), respectively. As in the previous example, we assume no external disturbances ($\dot{z}_1^m = 0$). The energy-based FBLC gains are selected as,

$$K_1 = K_2 = 10,$$

while the energy-based SMC method uses,

$$M_o = 10, \quad M_1 = 1$$

Figure 10 shows system responses under energy-based FBLC (in red) and SMC (in green). Both methods regulate generator frequency ω_1 to the nominal 377 rad/s, eliminating the steady-state error present under conventional governor control without requiring secondary control. They also produce smoother control trajectories, particularly in the valve position a_1 , which can reduce actuator wear and enhance operational longevity. Following the load variation around $t = 5$ s, the mechanical power output adjusts faster under energy-based control, while the conventional controller responds more slowly. Although tuning can improve the conventional response, it often increases overshoot and induces more aggressive transients. Overall, the energy-based controllers outperform the conventional approach in both transient and steady-state performance.

7 Conclusion

This paper extends prior work in energy space modeling by developing a multilayered distributed control framework that integrates physical and energy space representations of power systems components. By lifting component dynamics to energy space, the framework enables time-domain control design without phasor-based approximations or PQ decoupling. A key contribution is the extension to a third-order energy space model, where tangent space energy is treated as a state variable, improving control accuracy and physical interpretability. We pose a general distributed control problem and pro-

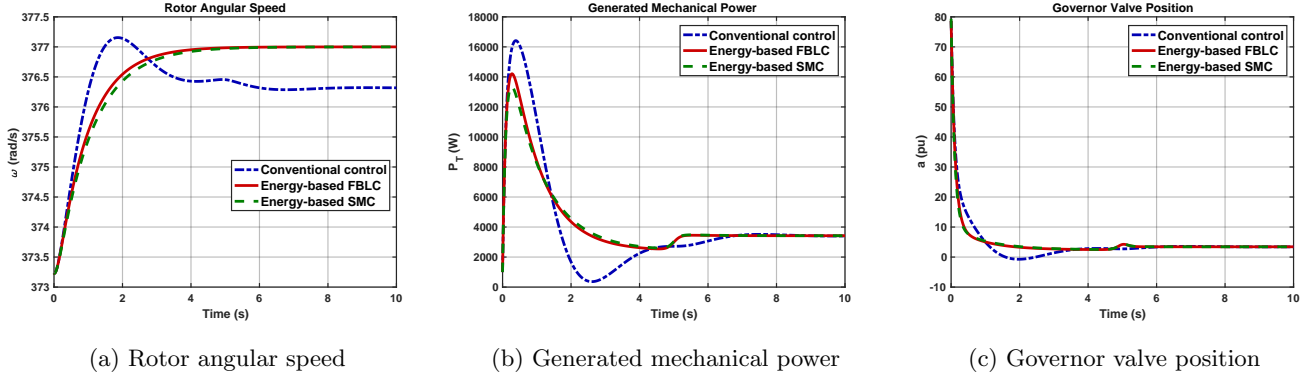


Fig. 10. System response of the synchronous generator under conventional governor control (29), energy-based FBLC, and energy-based SMC for a smooth step load, with the objective of stabilizing and regulating the rotor angular speed (frequency) ω_1 to 377 rad/s

pose two control designs, energy-based feedback linearizing control (FBLC) and sliding mode control (SMC), that use only local states and minimal neighbor information. Simulations on an RLC circuit and a synchronous generator demonstrate improved voltage and frequency regulation, respectively, in both transient and steady-state response. Future work includes developing hierarchical control architectures to translate system-level objectives into component-level references, extending the framework to MIMO systems, and incorporating time-varying parameters such as those in FACTS devices.

References

- [1] Federico Milano, Florian Dörfler, Gabriela Hug, David J. Hill, and Gregor Verbič. Foundations and challenges of low-inertia systems (invited paper). In *2018 Power Systems Computation Conference (PSCC)*, pages 1–25, 2018.
- [2] Jingyang Fang, Hongchang Li, Yi Tang, and Frede Blaabjerg. On the inertia of future more-electronics power systems. *IEEE Journal of Emerging and Selected Topics in Power Electronics*, 7(4):2130–2146, 2019.
- [3] Alessandro Crivellaro, Ali Tayyebi, Catalin Gavriluta, Dominic Gross, Adolfo Anta, Friederich Kupzog, and Florian Dörfler. Beyond low-inertia systems: Massive integration of grid-forming power converters in transmission grids. *2020 IEEE Power & Energy Society General Meeting (PESGM)*, pages 1–5, 2019.
- [4] Marija Ilić and John Zaborsky. *Dynamics and Control of Large Electric Power Systems*. Wiley, 2000.
- [5] Peter W Sauer and M A Pai. *Power System Dynamics and Stability*. Prentice Hall, 1998.
- [6] Marija Ilić, Rupamathi Jaddivada, and Xia Miao. Modeling and analysis methods for assessing stability of microgrids. *IFAC-PapersOnLine*, 50(1):5448–5455, 2017. 20th IFAC World Congress.
- [7] Rachid Darbali-Zamora and Eduardo I. Ortiz-Rivera. An overview into the effects of nonlinear phenomena in power electronic converters for photovoltaic applications. In *2019 IEEE 46th Photovoltaic Specialists Conference (PVSC)*, pages 2908–2915, 2019.
- [8] Sebastian A. Nugroho, Ahmad F. Taha, and Junjian Qi. Characterizing the nonlinearity of power system generator models. In *Proceedings of the American Control Conference (ACC)*, Philadelphia, PA, USA, 2019. arXiv preprint: <http://arxiv.org/abs/1902.06025>.
- [9] Xiuqiang He, Verena Häberle, Irina Subotić, and Florian Dörfler. Nonlinear stability of complex droop control in converter-based power systems. *IEEE Control Systems Letters*, 7:1327–1332, 2023.
- [10] D. Venkatramanan, M. K. Singh, O. Ajala, A. Domínguez-García, and S. Dhople. Integrated system models for networks with generators & inverters, 2022. arXiv preprint: <https://arxiv.org/abs/2203.08253>.
- [11] Brian B. Johnson, T. Roberts, O. Ajala, A. Domínguez-García, S. Dhople, D. Ramasubramanian, A. Tuohy, D. Divan, and B. Kroposki. A generic primary-control model for grid-forming inverters: Towards interoperable operation & control. *Hawaii International Conference on System Sciences*, 2022.
- [12] Uros Markovic, Ognjen Stanojev, Petros Aristidou, Evangelos Vrettos, Duncan Callaway, and Gabriela Hug. Understanding small-signal stability of low-inertia systems. *IEEE Transactions on Power Systems*, PP:1–1, 02 2021.
- [13] Xiaoyang Wang and Xin Chen. Distributed coordination of grid-forming and grid-following inverter-based resources for optimal frequency control in power systems. *arXiv preprint: https://arxiv.org/abs/2411.12682*, 2024.
- [14] Marija D. Ilić and Rupamathi Jaddivada. Multi-layered interactive energy space modeling for near-optimal electrification of terrestrial, shipboard and aircraft systems. *Annual Reviews in Control*, 45:52–75, 2018.
- [15] Marija D. Ilic and Rupamathi Jaddivada. Fundamental modeling and conditions for realizable and efficient energy systems. In *2018 IEEE Conference on Decision and Control (CDC)*, pages 5694–5701, 2018.
- [16] Marija Ilic and Rupamathi Jaddivada. Unified value-based feedback, optimization and risk management in complex electric energy systems. *Optimization and Engineering*, 21(2):427–483, 2020.
- [17] Milos Cvetkovic and Marija Ilic. Interaction variables for distributed numerical integration of nonlinear power system dynamics. In *2015 53rd Annual Allerton Conference on Communication, Control, and Computing (Allerton)*, pages 560–566, September 2015.

- [18] Xia Miao and Marija Ilic. High quality-of-service in future electrical energy systems: A new time-domain approach. *IEEE Transactions on Sustainable Energy*, 2020.
- [19] Marija Ilic, Xia Miao, and Rupamathi Jaddivada. Plug-and-play reconfigurable electric power microgrids, May 19 2020. US Patent 10,656,609.
- [20] Marija Ilic and Rupamathi Jaddivada. Toward technically feasible and economically efficient integration of distributed energy resources. In *2019 57th Annual Allerton Conference on Communication, Control, and Computing (Allerton)*, pages 796–803. IEEE, 2019.
- [21] Jan C. Willems. The behavioral approach to open and interconnected systems. *IEEE Control Systems Magazine*, 27(6):46–99, 2007.
- [22] P. Penfield, R. Spence, and S. Duinker. A generalized form of tellegen’s theorem. *IEEE Transactions on Circuit Theory*, 17(3):302–305, 1970.
- [23] Dimitri Jeltsema and Jacquélien M.A. Scherpen. Multidomain modeling of nonlinear networks and systems. *IEEE Control Systems Magazine*, 29(4):28–59, 2009.
- [24] J.L. Wyatt and M. Ilic. Time-domain reactive power concepts for nonlinear, nonsinusoidal or nonperiodic networks. In *IEEE International Symposium on Circuits and Systems*, pages 387–390 vol.1, 1990.
- [25] Rupamathi Jaddivada and Marija D. Ilic. A feasible and stable distributed interactive control design in energy state space. In *2021 60th IEEE Conference on Decision and Control (CDC)*, pages 4950–4957, 2021.
- [26] M. Ilic and X. Liu. A simple structural approach to modeling and analysis of the interarea dynamics of the large electric power systems: Part i—linearized models of frequency dynamics. In *North American Power Symposium*, pages 560–569, 1993.
- [27] Rupamathi Jaddivada, Sruthi Davuluri, Magnus Korpaas, and Marija Ilic. Recursive algorithm for resource allocation in radial network systems. In *2019 8th Mediterranean Conference on Embedded Computing (MECO)*, pages 1–4, 2019.
- [28] Hassan K. Khalil. *Nonlinear Systems*. Prentice Hall, Upper Saddle River, NJ, 3rd edition, 2002.
- [29] Michele Cucuzzella, Krishna Chaitanya Kosaraju, and Jacquélien Scherpen. Voltage control of dc networks: robustness for unknown zip-loads. *arXiv preprint: <https://arxiv.org/abs/1907.09973>*, 2019.